TECHNICAL NOTES

Natural convection in a rectangular enclosure with partial heating of the lower surface: experimental results

J. D. NICOLAS

Department of Mechanical Engineering and Applied Mechanics, University of Pennsylvania, Philadelphia,
PA 19104, U.S.A.

and

M. W. NANSTEEL

Department of Mechanical and Aerospace Engineering, Florida Institute of Technology, Melbourne,
FL 32901, U.S.A.

1. INTRODUCTION

NATURAL convection due to differential heating of the vertical walls in rectangular enclosures has been well-studied in part because of the wide range of important applications relevant to this phenomenon. However, relatively little attention has been given to the case of differential heating of both the horizontal and vertical surfaces of the enclosure. Such a circumstance arises for example when solar radiation, passing through a large window, is incident on the floor of a room. That portion of the floor which receives the radiation attains a temperature relatively greater than the cool window surface, resulting in buoyancy induced motion characterized by Rayleigh numbers in the approximate range 10^{10}–10^{12}. It appears that the only systematic study with respect to partial heating on the lower surface of an enclosure is due to November and Nansteel [1]. November and Nansteel theoretically examined the case of a square enclosure with isothermal cooling on one vertical wall and partial heating (isothermal) on the lower surface. The remainder of the enclosure boundary was insulated. Special attention was given to the heat transfer and flow structure in the vicinity of the flux singularity on the lower surface where the thermal boundary condition changes abruptly. It is demonstrated in ref. [1] that while local heat flux in the neighborhood of the flux singularity is unbounded, the integrated energy flow is finite in the same way as described by Bassani *et al.* [2] for pure conduction. Convective heat transfer is found [1] to increase monotonically with length of the heated section on the lower surface while the Nusselt number (ratio of total heat transfer to pure conduction heat transfer) is a maximum when approximately 60% of the lower surface is insulated and decays toward unity as the length of the heated section either approaches zero size or spans the entire lower surface. Kirkpatrick and Bohn [3] experimentally studied the flow structure and heat transfer in a cubical enclosure with various isothermal heating and cooling conditions imposed on the boundaries, e.g. isothermally heated lower surface and isothermal cooling of the adjacent vertical surfaces and the upper horizontal surface. Heat transfer data were obtained for Rayleigh numbers of order 10^{10} using water as the working fluid. Partial heating of the enclosure surfaces was not considered. Other studies [4–12] of buoyancy-induced convection featuring heating and cooling of non-parallel surfaces are reviewed by November and Nansteel [1].

The present work focuses on the convection inside a square

enclosure in which a portion of the lower surface is heated with a uniform heat flux while one vertical boundary is isothermally cooled, cf. Fig. 1. This configuration is investigated experimentally using water as the working fluid in the Rayleigh number range $7.29 \times 10^{10} < Ra < 3.69 \times 10^{11}$ which is of direct significance with regard to the passive heating of rooms via solar irradiation as discussed above. Results are obtained for the cases $l/L = \varepsilon = 1/3,\ 1/2,\ 2/3$. Heat transfer rate from the heated to the cooled surface of the enclosure is measured as a function of ε and Ra while the flow structure is studied via laser-illumination streak photography.

Nondimensionalization of the equations governing mass, momentum and energy indicate an essential dependence on the parameters Ra, Pr and ε, cf. Nicolas [13]. The average temperature of the heated surface, $\bar{T}_h$, is given by

$$\bar{T}_h - \bar{T}_c = \frac{q_h L}{k} \frac{1}{1-\varepsilon} \int_0^{1-\varepsilon} T(x,0)\, \mathrm{d}x. \qquad (1)$$

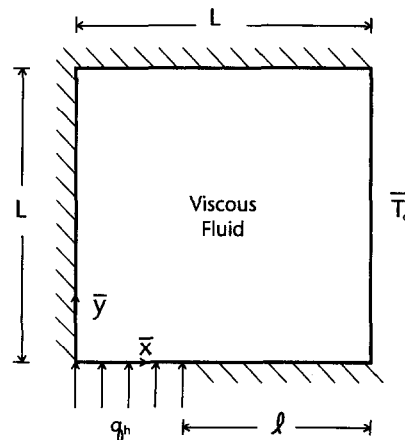The average heat flux on the cold wall is

$$q_c = q_h(1-\varepsilon) \qquad (2)$$

FIG. 1. Enclosure configuration and thermal boundary conditions.

NOMENCLATURE

g	gravitational acceleration [m s^{-2}]		$\bar{x}$	position coordinate [m]
k	thermal conductivity [W m^{-1} K^{-1}]		y	dimensionless position coordinate, $\bar{y}/L$
l	length of unheated section on lower surface [m]		$\bar{y}$	position coordinate [m].
L	enclosure side length [m]			
Pr	Prandtl number, v/α		Greek symbols	
q	average heat flux [W m^{-2}]		α	thermal diffusivity [m^2 s^{-1}]
q''	local heat flux [W m^{-2}]		β	coefficient of thermal expansion [K^{-1}]
Q	dimensionless heat flux, equation (3)		ε	dimensionless length of insulated portion of lower surface, l/L
$\bar{Q}$	heat transfer rate [W]		v	kinematic viscosity [m^2 s^{-1}]
Ra	Rayleigh number, $g\beta q_{\mathrm{h}}L^4/v\alpha k$ [1].		ρ	density [kg m^{-3}].
Ra^*	Rayleigh number used in ref. [1], $g\beta L^3(\bar{T}_{\mathrm{h}}-\bar{T}_{\mathrm{c}})/v\alpha$			
T	dimensionless temperature, $(\bar{T}-\bar{T}_{\mathrm{c}})k/q_{\mathrm{h}}L$		Subscripts	
$\bar{T}$	temperature [K]		c	cold surface
x	dimensionless position coordinate, $\bar{x}/L$		h	hot surface.

and the dimensionless heat transfer rate for this surface is

$$Q_{\mathrm{c}} = Q_{\mathrm{c}}(Ra, Pr, \varepsilon) = \frac{q_{\mathrm{c}}L}{k(\bar{T}_{\mathrm{h}}-\bar{T}_{\mathrm{c}})}. \qquad (3)$$

2. EXPERIMENTAL APPARATUS

The experimental test cell measures 15.2 cm square by 61 cm in depth and is constructed of 1.57 mm thick stainless steel sheet ($\bar{x} = 0, \bar{y} = 0, L$) and a 2.51 cm thick aluminum cooling manifold ($\bar{x} = L$). The end walls are made of 0.95 cm thick optical glass and 1.25 cm thick plexiglass. Boundary heating is accomplished through resistance heating strips bonded to the surface $\bar{y} = 0$. Average temperature of the heated surface $\bar{T}_{\mathrm{h}}$ is computed from equation (1) using 28 thermocouples mounted in small wells on the dry side of the lower surface. Measurement of the water-cooled cold surface temperature is accomplished in a similar way. Laser illumination streak photography is used to visualize the flow. Uncertainties in measurement of Ra and Q_{c} due to uncertainties in temperature and heat transfer measurement and fluid properties are $\pm 5\%$ and $\pm 10\%$ respectively. Further description of the experimental apparatus and procedure may be found in ref. [13].

3. RESULTS AND DISCUSSION

Experimental results for buoyancy-induced flow in the enclosure with $\varepsilon = 1/3, 1/2$ and $2/3$ are obtained in the range $7 \times 10^{10} < Ra < 4 \times 10^{11}$. Flow visualization results are presented and discussed for the cases $\varepsilon = 1/3$ and $1/2$ along with the heat transfer results.

Flow visualization

Particle visualization experiments reveal the natural convection flow to be laminar and mostly steady. The qualitative features of the flow structure are observed to be the same for each value of ε studied. The nominal flow structure consists of a central core region surrounded by boundary layers adjacent to the enclosure periphery. The peripheral boundary layer is nonuniform in both thickness and nominal velocity with respect to location on the boundary. The narrowest portion of the boundary layer and that with the greatest velocity is found adjacent to the cooled vertical surface $\bar{x} = L$. This result is not surprising since the surface $\bar{x} = L$ is the only vertical diabatic boundary. This behavior is also observed in the calculational results of November and Nansteel [1] for partial heating (isothermal) of the lower surface in the Rayleigh number range $10^3 \leqslant Ra^* \leqslant 10^6$. The core region in the present configuration exhibits rather large eddies, with velocities of generally lesser magnitude compared with the boundary layer flow. The eddy structures are

not entirely steady as they are observed to undergo small changes in size, shape and location within the core. Figure 2 shows a pair of large counter-rotating eddies in the upper left central core region for the case $\varepsilon = 1/3$, $Ra = 3.43 \times 10^{11}$. The eddy nearest the unheated vertical surface (in the left-hand central portion of Fig. 2) exhibits rotation in the clockwise sense as is consistent with the driving shear due to the adjacent rising boundary layer on the surface $\bar{x} = 0$. These core eddies are not predicted by the calculations of November and Nansteel [1] or Anderson and Lauriat [5] for heating from below and side cooling, however, the appearance of secondary rolls in the core of rectangular, differentially heated enclosures has been observed for large Rayleigh number. For example, secondary motions in the core were observed by Simpkins and Dudderar [14] for $Pr \geqslant 10$ and Rayleigh numbers of order 10^6 or greater. Also of note in Fig. 2, a portion of the rather thick boundary layer on the lower surface is visible. Note that heating occurs only over the section $0 \leqslant \bar{x} \leqslant \frac{2}{3}L$ on the enclosure lower boundary for the case of Fig. 2 and this appears to have little visible influence on the nature of the boundary layer adjacent to this surface. In fact no noticeable variation in basic flow structure was observed with changing ε in the range $1/3 \leqslant \varepsilon \leqslant 2/3$. It is important to note that the present observations support the speculation of November and Nansteel [1] and the observations of ref. [5] that the heated surface boundary layer remains attached to the surface $\bar{y} = 0$ despite the unstable density stratification in this layer even for Rayleigh numbers in the range $Ra = O(10^{11})$. Perhaps the pressure defect created near the corner $\bar{x} = \bar{y} = 0$ by the rising boundary layer along $\bar{x} = 0$ serves to stabilize this layer as suggested in ref. [5]. Figure 3 shows the lower right hand quadrant ($\bar{x} \gtrsim 1/2, \bar{y} \lesssim 1/2$) of the enclosure for the case $\varepsilon = 1/2$, $Ra = 2.98 \times 10^{11}$. In this figure the strong downflow in the boundary layer adjacent to the cold wall as well as entrainment into this layer from the core region is visible. Immediately downstream of the location where this layer is turned in the corner $\bar{x} = L, \bar{y} = 0$, a small region of separation is observed on the lower surface in Fig. 3. The separated layer is seen to undergo reattachment a short distance downstream of this corner. Also a small, rather weak eddy with clockwise recirculation can be observed just above this separation region, cf. Fig. 3. These flow features are in good agreement with streamline contours reported by November and Nansteel [1]. In ref. [1], for $Ra^* = 10^6$, the wall layer undergoes rapid thickening on the lower surface just downstream of the corner $\bar{x} = L, \bar{y} = 0$ and then gradually thins in the downstream direction. Similar behavior is predicted by the calculations of Anderson and Lauriat [5]. This behavior may be due to the rapid deceleration in the vertical boundary layer near the corner $\bar{x} = L, \bar{y} = 0$ which results in streamline divergence for moderate Ra and temporary
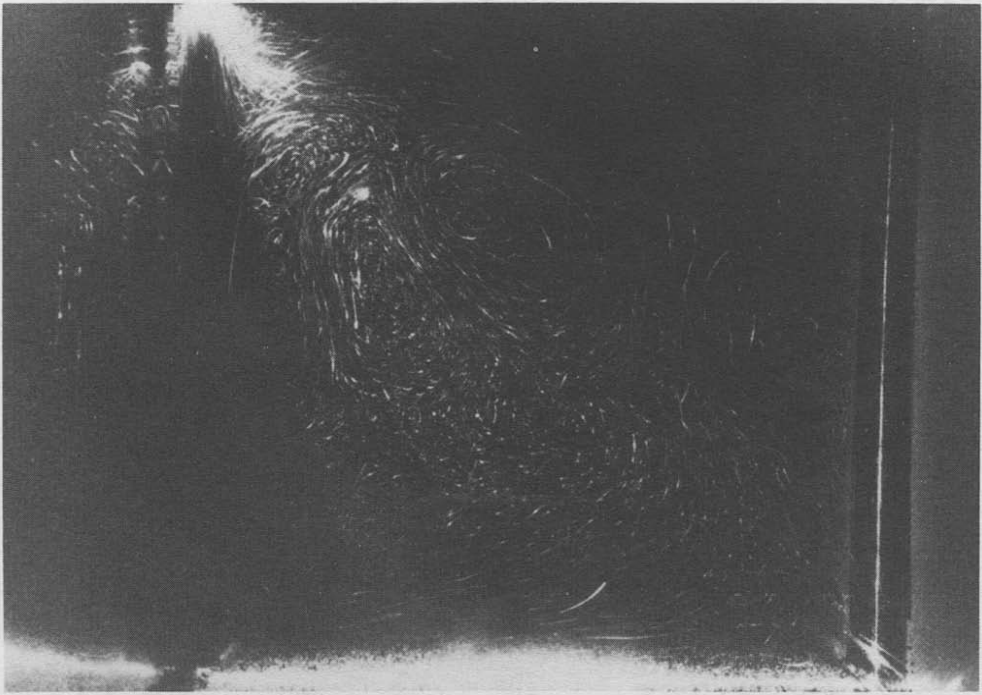
FIG. 2. Streak visualization photograph of main core eddies and lower surface boundary layer for $\varepsilon = 1/3$, $Ra = 3.43 \times 10^{11}$, exposure time = 15 s.
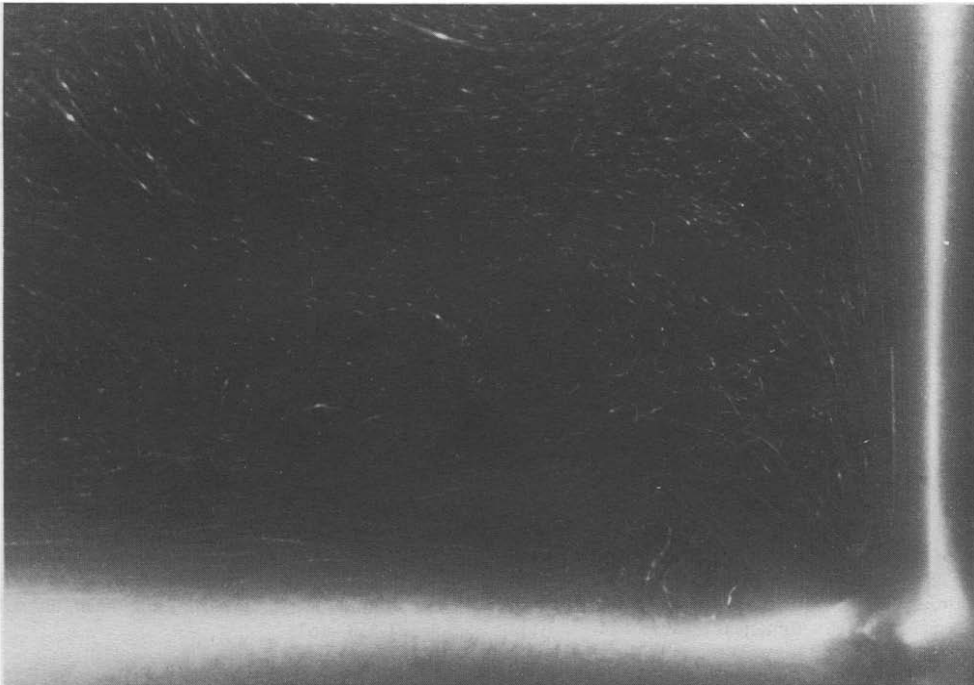

FIG. 3. Streak visualization photograph of corner region $\bar{x} = L, \bar{y} = 0$ showing boundary layer separation and reattachment for $\varepsilon = 1/2$, $Ra = 2.98 \times 10^{11}$, exposure time = 8 s.

Table 1. Heat transfer data, $\varepsilon = 1/3$

Ra	Pr	Q_c	$\bar{Q}_h$ (W)	$\bar{Q}_c$ (W)	$(\bar{Q}_h - \bar{Q}_c)/\bar{Q}_h$ (%)	$\bar{T}_h$ (°C)	$\bar{T}_c$ (°C)	$\bar{T}_h - \bar{T}_c$ (°C)
1.10×10^{11}	4.6	37.9	232	228	1.6	45.3	29.4	15.9
8.87×10^{10}	5.3	29.6	246	251	1.9	41.5	19.4	22.1
1.71×10^{11}	4.2	37.9	315	312	0.9	52.1	30.6	21.5
1.41×10^{11}	5.2	40.9	370	374	1.1	43.7	19.8	23.9
2.30×10^{11}	4.0	42.1	400	407	1.8	55.4	30.9	24.5
3.18×10^{11}	3.7	42.1	478	473	1.0	62.3	32.3	30.0
2.09×10^{11}	4.1	44.4	501	500	0.2	48.8	19.0	29.8
3.43×10^{11}	3.7	45.5	515	510	1.0	63.3	32.4	30.9

separation for large Ra as a consequence of the strong adverse pressure gradient. The structure reported in the present experiments, however, is rather distinct from the structure observed by Kimura and Bejan [4] for the case of isothermal heating on one vertical wall and isothermal cooling on the lower horizontal surface. In this case the core is more stably stratified, resulting in a weaker single cell circulation centered near the differentially heated corner.

Heat transfer

Heat transfer results for the case $\varepsilon = 1/3$ are shown in Table 1. Note that fractional heat losses $(\bar{Q}_h - \bar{Q}_c)/\bar{Q}_h$, are less than 2% for this case and less than 3% for the experiments overall. The data are well correlated by

$$Q_c = 1.65(1-\varepsilon)^{4/5} Ra^{0.135} \qquad (4)$$

and hence the results exhibit a modest trend of increasing Q_c with increasing Ra. The correlation of Pera and Gebhart [15] for a uniformly heated, isolated flat horizontal plate, when expressed in terms of Q and Ra, yields the quite similar result $Q = 0.70 Ra^{1/6}$ when the ambient fluid temperature is replaced by $\bar{T}_c$. This is remarkable in light of the fact that in the enclosure the boundary layer is turned in the corner $\bar{x} = L, \bar{y} = 0$, it then separates, reattaches and then flows over the unheated section $1 - \varepsilon < \bar{x}/L < 1$ while for the horizontal isolated plate, hydrodynamic growth and heating begin simultaneously at the plate leading edge. The minor dependence of these results on Ra indicates the relative weakness of horizontal buoyancy induced flows compared with purely vertical flows as in the case of the vertical isolated flat plate or the differentially heated vertical cavity. The dependence exhibited by equation (4) is also rather distinct from the dependence observed for horizontal layers heated from below ($Q \sim Ra^{1/3}$) due to the cellular nature of the flow in that case. The important effect of ε is best observed by using equation (2) in equation (4) which yields

$$\frac{q_h L}{k(\bar{T}_h - \bar{T}_c)} = 1.65(1-\varepsilon)^{-1/5} Ra^{0.135} \qquad (5)$$

indicating that $\bar{T}_h - \bar{T}_c$ increases with decreasing ε for fixed q_h. That is, the average temperature of the heated surface increases with the length of the heated section for fixed q_h. This behavior is an expected consequence of thermal boundary layer development and the uniform flux condition, cf. [15].

Results of refs. [1, 4, 5] are plotted along with the present results in Fig. 4 where the abscissa is $Ra^* = g\beta L^3 (\bar{T}_h - \bar{T}_c)/\nu\alpha$. Extrapolation of the present data to the limit $\varepsilon = 0$ indicates agreement with the numerical results of ref. [5] (uniform heating of the entire lower surface) that is well within 10% of Q_c. In this respect the present results and the calculations of ref. [5] serve to validate one another. Extrapolation of the low Rayleigh number isothermal surface numerical results of ref. [1] to values of $Ra^* = O(10^9)$ indicates, Fig. 4, that values of Q_c for the same value of Ra^* are similar for the two thermal boundary conditions (constant flux and isothermal). It is important to note that
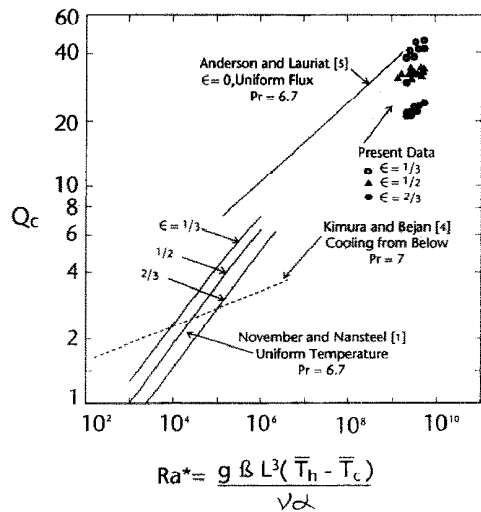

FIG. 4. Dimensionless heat transfer vs Ra^* including the results of [1, 4, 5].

this comparison is made on the basis of the same average temperature $\bar{T}_h$. With this in mind the coincidence of the heat transfer results for the two boundary conditions is completely consistent with the findings of Pera and Gebhart [15] for uniformly heated and isothermally heated isolated horizontal plates. Although the *local* value of Nusselt number, $q''(\bar{x})\bar{x}/k(\bar{T}(\bar{x}, 0) - \bar{T}_c)$, differs by 27% for the two conditions [15] it is easily shown from the correlations of ref. [15] that when the uniform flux surface has the same average temperature as the isothermal surface, the mean heat flux over the two surfaces differs by less than 8%. It is also important to note from Fig. 4 that the dependence of Q_c on ε is slightly stronger for the case of a uniform surface flux ($Q_c \sim (1-\varepsilon)^{3/4}$, with Ra^* fixed) than for the isothermal surface condition ($Q_c \sim (1-\varepsilon)^{3/5}$). Numerical results from Kimura and Bejan [4] for isothermal cooling of the lower surface are also plotted in Fig. 4. The weaker circulation for this configuration leads to significantly smaller heat transfer rates when compared with the present data for heating from below.

REFERENCES

1. M. November and M. W. Nansteel, Natural convection in rectangular enclosures heated from below and cooled along one side, *Int. J. Heat Mass Transfer* **30**, 2433–2440 (1987).
2. J. Bassani, M. Nansteel and M. November, Adiabatic-

isothermal mixed boundary conditions in heat transfer, *Int. J. Heat Mass Transfer* **30**, 903–909 (1987).

3. A. T. Kirkpatrick and M. Bohn, An experimental investigation of mixed cavity natural convection in the high Rayleigh number regime, *Int. J. Heat Mass Transfer* **29**, 69–82 (1986).

4. S. Kimura and A. Bejan, Natural convection in a differentially heated corner region, *Phys. Fluids* **28**, 2980–2989 (1985).

5. R. Anderson and G. Lauriat, The horizontal natural convection boundary layer regime in a closed cavity, *Proc. 8th Int. Heat Transfer Conf.*, San Francisco, California, pp. 1453–1458 ((1986).

6. K. Torrance and J. Rockett, Numerical study of natural convection in an enclosure with localized heating from below—creeping flow to the onset of laminar instability, *J. Fluid Mech.* **36**, 33–54 (1969).

7. K. E. Torrance, L. Orloff and J. A. Rockett, Experiments on natural convection in enclosures with localized heating from below, *J. Fluid Mech.* **36**, 21–31 (1969).

8. D. Greenspan and D. Schultz, Natural convection in an enclosure with localized heating from below, *Comput. Meth. Appl. Mech. Engng* **3**, 1–10 (1974).

9. P. Chao, H. Ozoe, S. Churchill and N. Lior, Laminar

natural convection in an inclined rectangular box with the lower surface half-heated and half-insulated, *J. Heat Transfer* **105**, 425–432 (1983).

10. G. Shiralkar and C. Tien, A numerical study of the effect of a vertical temperature difference imposed on a horizontal enclosure, *Numer. Heat Transfer* **5**, 185–197 (1982).

11. D. Poulikakos, Natural convection in a confined fluid filled space driven by a single vertical wall with warm and cold regions, *J. Heat Transfer* **107**, 867–876 (1985).

12. M. November, Natural convection in a rectangular enclosure heated and cooled on adjacent walls, M.S. Thesis, University of Pennsylvania, Philadelphia, Pennsylvania (1986).

13. J. D. Nicolas, Natural convection in a rectangular enclosure with partial heating of one surface, M.S. Thesis, University of Pennsylvania, Philadelphia, Pennsylvania (1991).

14. P. G. Simpkins and T. D. Dudderar, Convection in rectangular cavities with differentially heated end walls, *J. Fluid Mech.* **110**, 433–456 (1981).

15. L. Pera and B. Gebhart, Natural convection boundary layer flow over horizontal and slightly inclined surfaces, *Int. J. Heat Mass Transfer* **16**, 1131–1146 (1973).

Critical heat flux in pool boiling of binary mixtures as determined by the quenching method

JYH-FUH CHEN, MING-HUEI LIU and YU-MIN YANG†

Department of Chemical Engineering, National Cheng Kung University, Tainan, Taiwan 70101, R.O.C.

INTRODUCTION

THE CRITICAL heat flux (CHF) is the highest possible nucleate boiling heat flux. For a system in which the surface heat flux is controlled, CHF is the heat flux for which there is a sudden jump in surface temperature resulting from the increase of the heat flux. For a system in which the surface temperature is controlled, CHF is the heat flux for which the surface heat flux starts to decrease as a result of an incremental change in the surface temperature. The understanding and prediction of CHF is therefore very important in the design of heat exchange equipment operating in the nucleate boiling regime. The need to understand and predict the CHF in mixtures has been driven by the ubiquitous presence of mixtures in the chemical and process industries.

A dilemma of CHF in binary mixtures is that some investigators found out for certain compositions the CHF was as much as twice the value for either pure component, but on the other hand, critical heat fluxes were found to be always between those of the pure components by different investigators. This dilemma of CHF in binary mixtures may be shown schematically by Fig. 1, which appeared originally in Collier's book [1].

As shown in Fig. 2, the bewildering status of the critical heat flux for the acetone–water binary mixture system is obvious. In this figure, $q_{c,1}$ is the ideal linear mixing law critical heat flux defined as

$$q_{c,1} = (1-x)q_{c,1} + xq_{c,2} \tag{1}$$

where $q_{c,1}$ and $q_{c,2}$ are the critical heat fluxes for pure component 1 and pure component 2, respectively, and x is the mass fraction of component 2 in the binary liquid mixture.

It is worthy to note that the heating surfaces used by van Wijk *et al.* [2], Carne [3] and Stephen and Preußer [4] are 0.2 mm platinum wire, 3.2 mm stainless steel tube, and 14 mm nickel tube, respectively. These results revealed that the dilemma suffered seemingly because the influential roles of geometry and of geometric scale on CHF had not yet been identified or properly diagnosed.

Increased critical heat flux

The well-known effect that the CHF with small diameter wires increases with concentration of a volatile organic component to a maximum value and then decreases has been noted by van Stralen and coworkers and many other investigators. Van Stralen [5, 6] defined the CHF in terms of a bubble-packing model. Since the bubble departure diameter decreases to a minimum at the same composition as the minimum bubble growth rate, van Stralen surmised that the increase he observed in CHF was due to the higher bubble-packing density possible in the mixtures. This is an interesting coincidence, termed the 'boiling paradox', whereby the maximum CHF occurs at the minimum bubble growth rate and departure diameter. The increase in the CHF is then explained by the summation of the contributions of direct vaporization at the heated surface and the convective heat transfer caused by the bubble motion. Van Stralen showed that while the evaporation heat flux decreased with the addition of a volatile solvent to water, the convective heat flux increased by a greater margin. Thus CHF experienced an increase in the mixture in comparison to pure water.

Yang and Maa [7] explained qualitatively the maximum in CHF as being due to three intercorrelated phenomena. The first is the slowing down in bubble growth rate caused by the exhaustion of the more volatile component near the

---

† Author to whom correspondence should be addressed.